

Statistical properties of eigenstate amplitudes in complex quantum systems

Wouter Beugeling,^{1,2,3} Arnd Bäcker,^{1,4} Roderich Moessner,¹ and Masudul Haque^{1,5}

¹Max-Planck-Institut für Physik komplexer Systeme, Nöthnitzer Straße 38, 01187 Dresden, Germany

²Lehrstuhl für Theoretische Physik I & II, Technische Universität Dortmund, Otto-Hahn-Straße 4, 44221 Dortmund, Germany

³Physikalisches Institut, Universität Würzburg, Am Hubland, 97074 Würzburg, Germany

⁴Technische Universität Dresden, Institut für Theoretische Physik and Center for Dynamics, 01062 Dresden, Germany

⁵Department of Theoretical Physics, Maynooth University, Co. Kildare, Ireland

(Dated: November 18, 2021)

We study the eigenstates of quantum systems with large Hilbert spaces, via their distribution of wavefunction amplitudes in a real-space basis. For single-particle ‘quantum billiards’, these real-space amplitudes are known to have Gaussian distribution for chaotic systems. In this work, we formulate and address the corresponding question for many-body lattice quantum systems. For integrable many-body systems, we examine the deviation from Gaussianity and provide evidence that the distribution generically tends toward power-law behavior in the limit of large sizes. We relate the deviation from Gaussianity to the entanglement content of many-body eigenstates. For integrable billiards, we find several cases where the distribution has power-law tails.

I. INTRODUCTION

Except for particularly simple systems, eigenstates of quantum Hamiltonians are complex objects, described by an exponentially large number of coefficients (amplitudes). Energy eigenstates are constitutive to the formulation of quantum mechanics. They are also essential in describing closed quantum systems, e.g., in considerations of thermalization [1–5]. Thus, one might reasonably regard the structure of eigenstates, e.g., the statistical properties of amplitudes, as being fundamental to our understanding of the quantum world. Amplitude distributions have been studied for single-particle (quantum billiard) systems [6–14]. However, little is known about corresponding distributions for quantum many-body Hamiltonians. In this work we address distributions of coefficients (in the basis of real-space configurations), clarifying in particular the consequences of *integrability*.

While it is difficult to find a universally accepted definition of quantum integrability [15, 16], we will refer to systems with Poissonian level spacing statistics (within a single symmetry sector) to be integrable or regular, and to those with random-matrix statistics as non-integrable or chaotic. This distinction appears both in single-particle billiards [17, 18] and in many-body systems [19–30]. This operational definition is inadequate in some situations, but will suffice for this work. Many-body integrable systems include non-interacting (‘free’) fermions, free bosons, and systems solvable by Bethe ansatz. Integrable quantum billiards are those whose corresponding classical problems have as many independent conserved quantities as degrees of freedom. Some further comments on integrability are provided in Appendix A.

For quantum billiard systems, the distribution of real-space amplitudes $\psi(\vec{x}) = \langle \vec{x} | \psi \rangle$ of eigenstates has been studied both for chaotic and for mixed systems [6–12, 14, 31]. In the chaotic case the amplitude distribution is expected to be Gaussian for almost all eigenstates (with some possible exceptions [32, 33]). This follows from the conjecture that high-energy eigenstates of chaotic billiards resemble random superpositions of many plane waves leading to a Gaussian distribution by the central limit theorem [7, 34]. For single-particle sys-

tems, the particle position is the natural basis in which to express the amplitudes. In the many-body case, the choice of basis is less obvious, but a direct generalization is the basis of many-body configurations in real space. For lattice systems, this is also a widely used basis for numerical diagonalization. Our study focuses on coefficients in this basis.

For *non-integrable* systems, we show that eigenstates away from spectral edges have Gaussian coefficient distributions. The resemblance to Gaussian form improves with increasing deviation from integrability, and also improves systematically with system size. For *integrable* many-body systems, there is clear deviation from Gaussian shape. We provide evidence that the distribution approaches a power law as the size is increased. The convergence is extremely slow — a meaningful scaling analysis could only be performed for free fermions, but data for several integrable systems show the same trend. An analytic argument is constructed for a toy model of distinguishable particles, which accounts for the power-law form and the slow convergence. The presented numerical data and arguments, taken together, naturally lead to the conjecture that eigenstates of integrable many-body systems generically have power-law coefficient distributions in the large-size (‘thermodynamic’) limit. This conjecture is remarkable because ‘generic’ results are usually expected for chaotic rather than integrable systems.

We relate the coefficient distribution to the *entanglement entropy* between two spatial partitions. We show that larger deviations from Gaussian shape correlate strongly with low entanglement, and provide intuition for this correlation.

We also present some results for integrable quantum billiard systems. Explicit calculation shows in a few cases that the amplitude distributions have power-law tails. An extended power-law region can appear when the regular eigenfunctions contain many inequivalent peaks. The feature is intriguing but is not present in all integrable billiard systems.

This article is structured as follows. In Sec. II, we introduce the many-body models and present a general study of their coefficient distributions, highlighting the differences between non-integrable and integrable many-body systems, the deviation from Gaussianity and the correlation of this deviation with the entanglement entropy. In Sec. III, we focus

on integrable many-body systems, and provide numerical evidence and argumentation supporting approach to power-law behavior in the large-size limit. In Sec. IV we consider several single-particle quantum billiard systems and present results on amplitude distributions for several integrable and weakly non-integrable billiards. Section V discusses the context and some implications of our results. We provide additional data and supporting discussions in the appendices.

II. MANY-BODY QUANTUM SYSTEMS

In this section, we introduce the many-body Hamiltonians we use in this paper (Sec. II A), and then present a general overview of the coefficient distributions (Sec. II B). The distributions are close to Gaussian away from the spectral edges in non-integrable systems. They deviate significantly from Gaussianity for many eigenstates in integrable systems, and for eigenstates at the spectral edges in all systems. In Sec. II C we quantify the deviation from Gaussianity using the Kullback-Leibler divergence, and investigate the degree of Gaussianity in various cases using this measure. We show that, with increasing system size, resemblance to Gaussian form improves for non-integrable systems but deteriorates for integrable systems.

A. Models

We consider the spin- $\frac{1}{2}$ XXZ and Bose-Hubbard systems, on finite one-dimensional chains. We use open boundary conditions to avoid complications due to translation symmetry. For the XXZ chain, a next-nearest-neighbor (NNN) coupling breaks integrability:

$$H_{\text{XXZ}} = \sum_{i=1}^{L-1} h_{i,i+1} + \lambda \sum_{i=2}^{L-2} h_{i,i+2}, \quad (1)$$

where $h_{i,j} = S_i^x S_j^x + S_i^y S_j^y + \Delta S_i^z S_j^z$ (with spin- $\frac{1}{2}$ operators $S_i^{x,y,z}$) and L is the number of sites. The NNN (second) term excludes the coupling between sites 1 and 3, breaking reflection symmetry for $\lambda \neq 0$. We use $\Delta = 0.8$ throughout this work.

The Bose-Hubbard chain is described by the Hamiltonian

$$H_{\text{BH}} = \sum_{i=1}^{L-1} (b_i^\dagger b_{i+1} + b_{i+1}^\dagger b_i) + \lambda \sum_{i=1}^L b_i^\dagger b_i^\dagger b_i b_i, \quad (2)$$

where b_i denotes the bosonic annihilation operator on site i .

The number N_\uparrow of ‘‘up’’ spins (XXZ) and the number of bosons N_b (Bose-Hubbard) are conserved quantities. We study a single sector at a time, i.e., we fix (L, N_\uparrow) or (L, N_b) . The Hilbert space dimensions are $D = \binom{L}{N_\uparrow}$ for the XXZ chain and $D = \binom{L+N_b-1}{N_b}$ for the Bose-Hubbard system.

In both Hamiltonians (1) and (2), the second term breaks integrability; the dimensionless parameter λ controls proximity to integrability. The two integrable ($\lambda = 0$) Hamiltonians are

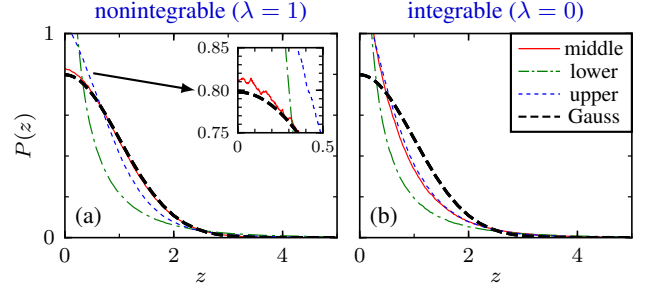


FIG. 1. (a) Amplitude distributions for non-integrable XXZ chain, with $(L, N_\uparrow) = (17, 8)$, $\Delta = 0.8$, and $\lambda = 1$. The distributions are over 250 eigenstates in the middle ($E \approx 0$), at the lower edge, and at the upper edge of the spectrum. The black dashed curve is the Gaussian distribution with unit variance. The inset shows a magnification near zero. (b) Same, for the integrable XXZ chain, with $\lambda = 0$.

the nearest-neighbor XXZ Hamiltonian, which is integrable by Bethe ansatz, and a chain of free (non-interacting) bosons, which is integrable due to the absence of interactions. We will present data mostly for $\lambda = 1$ (typical non-integrable case) and $\lambda = 0$ (integrable case).

In addition to the Hamiltonians classes (1) and (2), for our detailed treatment of integrable systems we will also consider a tight-binding system of N_f free fermions on an L -site chain,

$$H_{\text{FF}} = \sum_i (c_i^\dagger c_{i+1} + c_{i+1}^\dagger c_i) + \sum_i V_i c_i^\dagger c_i, \quad (3)$$

subject to a weakly varying potential V_i which leaves the system integrable but avoids lattice symmetries. Here c_i denotes the fermionic annihilation operator on site i . The Hamiltonian conserves the fermion number N_f . The Hilbert space dimension is $D = \binom{L}{N_f}$.

B. Gaussian and non-Gaussian distributions

We are interested in the statistics of coefficients $c_\gamma^{(\alpha)} \equiv \langle \phi_\gamma | \psi_\alpha \rangle$ of the energy eigenstates $|\psi_\alpha\rangle$. The basis states $\{|\phi_\gamma\rangle\}$ are spatial configurations, i.e., eigenstates of the local operators S_i^z or $b_i^\dagger b_i$. Normalization ensures that $\sum_{\gamma=1}^D |c_\gamma^{(\alpha)}|^2 = 1$. We study distributions of $z = |c_\gamma| \sqrt{D}$ (eigenstate indices α are suppressed). These distributions $P(z)$ then have unit variance, which simplifies comparison between different sizes.

In Fig. 1, we show the distributions of coefficients of 250 eigenstates, taken from the edges and from the middle of the spectra. States at the edge are special; they tend to be non-generic (‘‘integrable-like’’). In the coefficients this is manifested by non-Gaussian distributions, regardless of whether the system is integrable or not. For integrable many-body systems, e.g., the XXZ chain with $\lambda = 0$ [Fig. 1(b)] and other cases shown later, the distribution is also markedly non-Gaussian for eigenstates in the middle of the spectrum.

In contrast to the cases discussed above, for non-integrable systems (e.g., the XXZ chain with NNN coupling at $\lambda = 1$),

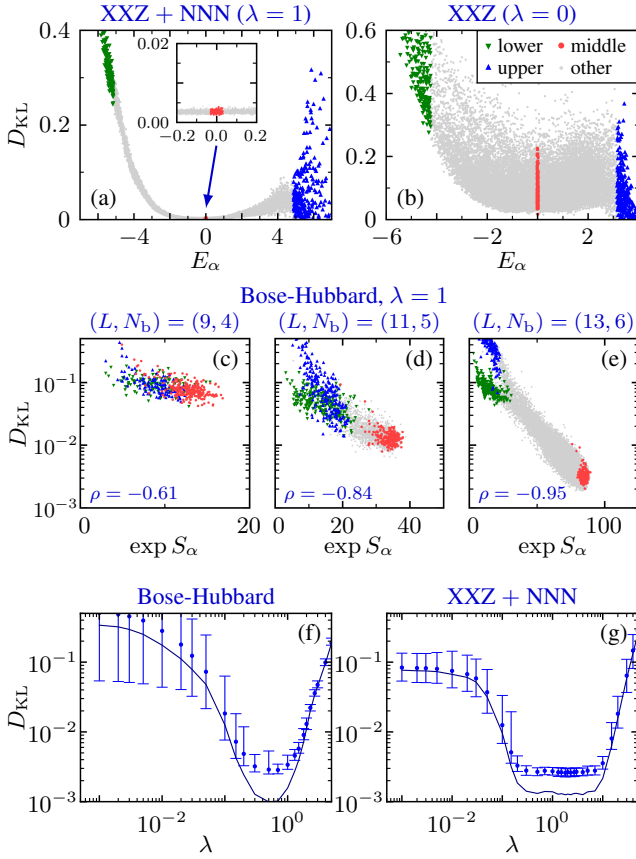


FIG. 2. Kullback-Leibler divergence D_{KL} (deviation from Gaussianity), using $(L, N_\uparrow) = (17, 8)$ for XXZ and $(L, N_b) = (13, 6)$ for Bose-Hubbard. (a) Per-eigenstate D_{KL} versus eigenenergy E_α for the XXZ chain ($\Delta = 0.8$) with and without NNN coupling. The highlighted states correspond to distributions shown in Fig. 1. (c)–(e) Per-eigenstate D_{KL} against exponentiated entanglement entropy for three system sizes of the Bose-Hubbard model. We indicate the Pearson correlation coefficient ρ . (f,g) D_{KL} as function of λ . Data points and error bars are average and standard deviation of the per-eigenstate D_{KL} values for 250 eigenstates in the middle of the spectrum. Solid line is D_{KL} of the distribution of all coefficients of these states together.

the distribution of the coefficients of the eigenstate in the middle of the spectrum has overall Gaussian behavior, see Fig. 1(a). The same is valid for the Bose-Hubbard chain with $\lambda \sim 1$ (not shown). A Gaussian $P(z)$ is expected for complex non-integrable Hamiltonians — it is equivalent to the Porter-Thomas distribution for $|z|^2$ in nuclear physics [35], and has been assumed or tested for condensed-matter Hamiltonians, e.g., in Ref. [36–39].

We observe a weak deviation from the Gaussian close to zero (Fig. 1, inset) The small excess weight near $z = 0$ is balanced at intermediate values of z —the distribution is lower than the Gaussian at intermediate z and then overshoots the Gaussian curve again at large z . The overall distribution thus has higher kurtosis than the Gaussian—about 3.17 for the data shown in Fig. 1(a). The deviation is characterized in some detail in the following subsection.

C. Deviation from Gaussianity

We will now present a quantitative analysis of deviation from “Gaussianity”. For this purpose we use a commonly used measure of the difference between two distributions, namely the Kullback-Leibler divergence (KLD) [40]. The KLD between $P(z)$ and the standard Gaussian distribution $P^G(z)$ is

$$D_{KL}(P||P^G) = \int_0^\infty P(z) \log \frac{P(z)}{P^G(z)} dz. \quad (4)$$

This quantity vanishes if $P(z)$ is identical to $P^G(z)$ and grows as $P(z)$ increasingly deviates from $P^G(z)$.

In Figs. 2(a,b), the KLD for each eigenstate is plotted against corresponding eigenenergies. Consistent with Fig. 1(a), in the non-integrable case [Fig. 2(a)], the D_{KL} values are close to zero in the middle and larger at the edges of the spectrum. In the integrable case [Fig. 2(b)], there is a large spread of D_{KL} throughout the spectrum.

This behavior is reminiscent of that of bipartite entanglement entropy (EE) S_α of eigenstates [41]: in integrable systems, the middle of the spectrum has both generic, high-EE eigenstates but also a substantial number of non-generic, low-EE eigenstates [42, 43], while non-integrable systems have only high-EE eigenstates in the middle of the spectrum [42, 44, 45]. This suggests that the KLD of an eigenstate is inversely correlated with EE, and that large KLD and small EE both represent deviations from generic (effectively-random or ‘thermal’) behavior.

The correlation between the KLD and EE is shown in Fig. 2(c)–(e), using scatter plots of the per-eigenstate KLD against the per-eigenstate exponentiated EE, $\exp(S_\alpha)$. Here the entanglement is between two spatially connected parts of the Bose-Hubbard chain, of sizes l and $l+1$, where $2l+1 = L$. The data exhibits a very significant correlation between the KLD and EE, with improving correlation for increasing system size. We quantify this correlation using Pearson correlation coefficients ρ between $\exp S_\alpha$ and $\log D_{KL}$, which measures how linear the correlation between these two quantities is. The coefficient is negative because larger-KLD states generally have smaller entanglement, i.e., the plots overall have negative slope. The magnitude of ρ increases steadily with system size. Similar behavior is observed for the XXZ model with NNN couplings (not shown), which suggests that the improvement of correlation with increasing system size is a generic feature.

The participation ratio (PR) of eigenstates in the real-space configuration basis is more directly correlated with the KLD. The inverse PR

$$p^{-1} = D \sum_\gamma |c_\gamma|^4 = \int z^4 P(z) dz \quad (5)$$

is the kurtosis of the coefficient distribution, having the value $p = 1/3$ for a Gaussian distribution. The (inverse) PR has been used as a characterization of proximity to integrability [5, 28, 42, 46].

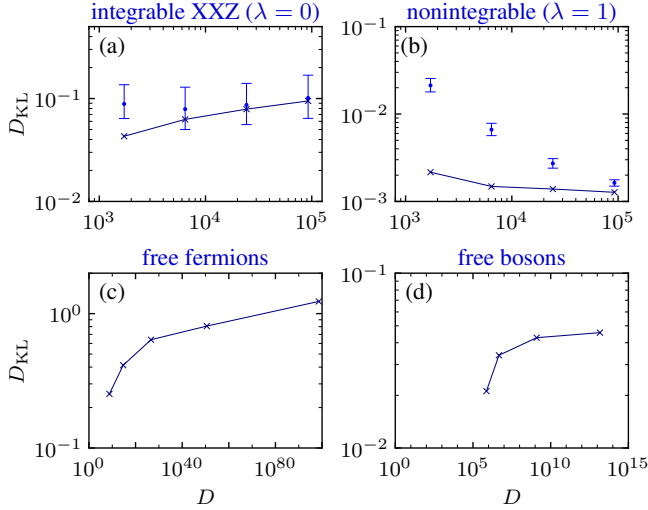


FIG. 3. Kullback-Leibler divergence D_{KL} as function of the system size (Hilbert space dimension D). (a,b) The XXZ chain ($\Delta = 0.8$) for 250 eigenstates in the middle of the spectrum. The data points (dots) and error bars indicate the average and standard deviation of the per-state KLD. The solid line (crosses) shows the D_{KL} values of the distribution of the coefficients of the 250 states taken together. (c,d) Eigenstate-averaged KLD for free fermions and free bosons, respectively.

Like the KLD, the PR can be calculated directly from the shape of the coefficient distribution; in contrast, the EE involves a partial trace which requires additional information about the spatial structure of the basis states. In view of the correlation between EE and KLD displayed in Figs. 2(c)–(e), it is thus expected that the EE and the PR should be positively correlated, as explored in Ref. [42]. We provide some further data in Appendix B.

Figures 2(f,g) show the KLD as a function of the integrability-breaking parameter λ . In the non-integrable regime ($\lambda \sim 1$) the coefficient distribution for every eigenstate in the middle of the spectrum is close to Gaussian, with D_{KL} near zero. For $\lambda \rightarrow 0$, the values of D_{KL} grow, and there is a large variation between the different eigenstates, reflecting the large spread of D_{KL} values in Fig. 2(b). For $\lambda \gg 1$, D_{KL} increases rapidly. In this limit, local conserved quantities divide the Hilbert space into uncoupled sectors, leading to a large number of zero coefficients, which accounts for the strong deviation from Gaussianity.

Figure 3 shows the KLD as a function of system size. The smallest and largest system sizes for the XXZ chain [Figs. 3(a,b)] correspond to $L = 13$ and 19. For the free-fermion and free-boson chains [Figs. 3(c,d)], the accessible sizes are much larger, because the coefficient distributions can be obtained without explicit numerical diagonalization of the many-body Hamiltonians, using the fact that each many-body eigenstate is built out of single-particle eigenstates as a single Slater determinant (non-interacting fermions) or as a single permanent (non-interacting bosons). The issue is discussed further in Sec. III A.

In the non-integrable XXZ chain [Fig. 3(b)], there is a clear

decrease of D_{KL} (increasing Gaussianity) with increasing system size. For the integrable cases, both the integrable XXZ chain and the non-interacting systems, D_{KL} increases with system size, meaning that $P(z)$ becomes less Gaussian. This is consistent with our conjecture in the next section that $P(z)$ approaches a power law in the large-size limit. In addition, relatively large fluctuations between the eigenstates are observed [error bars in Fig. 3(a)], reflecting the broad distribution seen in Fig. 1(b). This is consistent with the idea that eigenstates of integrable systems have a non-universal structure at finite sizes.

III. INTEGRABLE MANY-BODY SYSTEMS

We now concentrate on integrable systems and consider the coefficient distribution in the limit of large sizes. First, we describe the numerical analysis that leads to the conjecture of power-law behavior at large sizes (Sec. III A). The rest of the section provides a series of analytical arguments in support of this conjecture.

A. Numerical analysis

The eigenstate coefficients for free bosons and free fermions can be evaluated without explicit diagonalization of the many-body Hamiltonian, using the fact that the many-body eigenstates are built out of single-particle eigenstates. The eigenstates are chosen by drawing the ‘momenta’ k_j randomly such that the many-body energies lie in the desired energy range. For larger Hilbert spaces, we typically sample 10^3 – 10^4 coefficients of each eigenstate. For free fermions, the eigenfunctions are (Slater) determinants, which can be evaluated efficiently, allowing us to sample relatively large systems (> 300 sites). For the XXZ chain, we are limited to exact diagonalization and the sizes are modest (≈ 20 sites). Intermediate are free bosons (> 30 sites), whose eigenfunctions are permanents, whose numerical evaluation is less favorable than determinants.

Figures 4(a,b,c) present double-logarithmic plots of the coefficient distribution for three integrable systems. A power-law behavior would show up as a straight line in this representation. The data in the free fermionic case shows a clear evolution toward power-law behavior as the system size is increased. The trend in the other two systems is in the same direction, but less pronounced, presumably because of limited system sizes. The data is further analyzed in Figs. 4(d,e,f) through the slope of the curve in the double-logarithmic plot,

$$\frac{d \log P}{d \log z} = \frac{z}{P} P'(z), \quad (6)$$

the double-logarithmic derivative. Power-law behavior of P would imply a constant (flat) double-logarithmic derivative, its value giving the power-law exponent. The inset shows that the slope of the double-logarithmic derivative in logarithmic

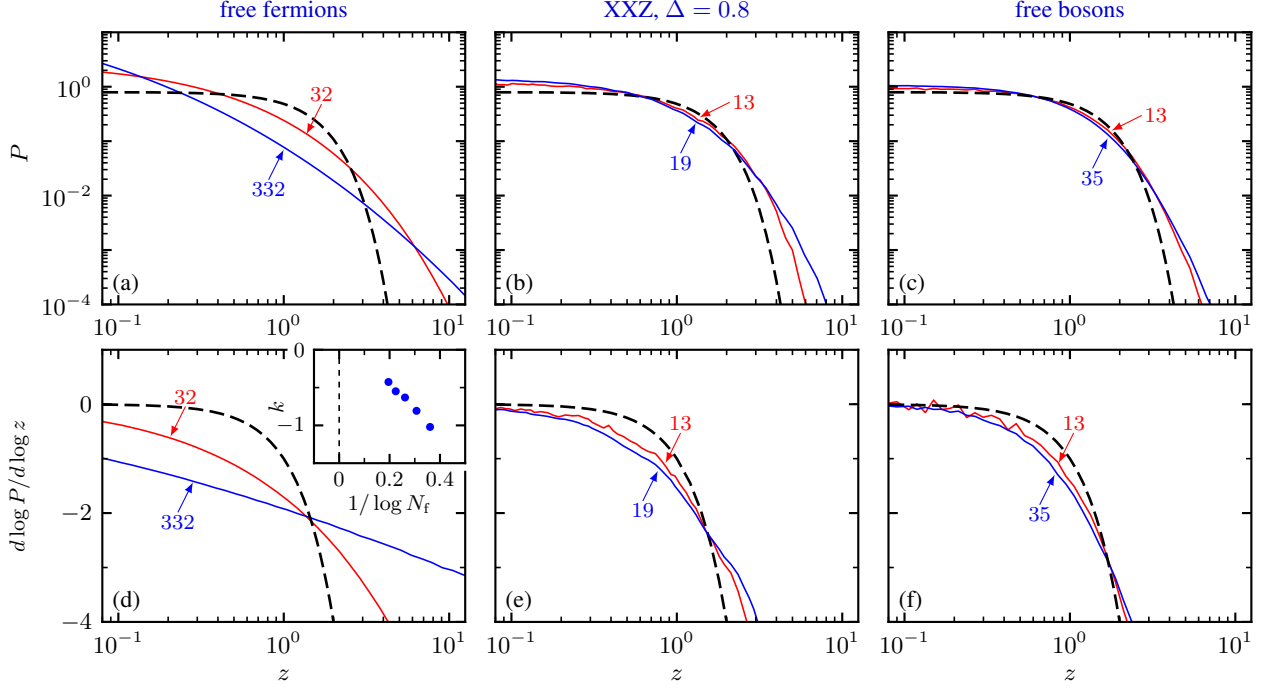


FIG. 4. (a–c) Amplitude distributions for integrable many-body systems, sampled from multiple eigenstates in the middle of the spectrum. Dashed curves are Gaussians. (a) Free-fermion chain; $(L, N_f) = (32, 16)$ and $(332, 166)$, ($D \sim 10^8$ and 10^{98}). (b) XXZ chain at $\Delta = 0.8$, with $(L, N_f) = (13, 6)$ and $(19, 9)$ ($D = 1716$ and 92378). (c) Free-boson chain; $(L, N_b) = (13, 6)$ and $(35, 17)$ ($D \sim 10^4$ and 10^{13}). (d–f) Corresponding double-logarithmic derivatives. Inset in (d) is the “curvature” $k = \frac{d^2 \log P}{d(\log z)^2}$ as function of $1/\log N_f$ for the free-fermion chain.

scale,

$$k = \frac{d^2 \log P}{d(\log z)^2}, \quad (7)$$

becomes smaller, arguably scaling to zero, in the large-size limit $N_f \rightarrow \infty$. The available sizes do not allow a meaningful extrapolation for the other two systems, but show the same general trend. This observation, together with further supporting arguments below, lead to the conjecture that the tails of the coefficient distributions of eigenfunctions of integrable many-body systems approach power-law shapes in the large-size limit.

B. Structure of the many-body coefficients

A common feature of several types of integrable systems is that many-body eigenstates can be constructed out of single-particle eigenstates. For example, a two-particle wavefunction is of the form $\phi_a(1)\phi_b(2) \mp \phi_a(2)\phi_b(1)$ for fermions and bosons and of the form $\phi_a(1)\phi_b(2) + e^{i\chi}\phi_a(2)\phi_b(1)$ for the XXZ chain, where χ is a phase shift and $\phi_{a,b}$ are single-particle eigenstates. We now consider the structure of the many-body coefficients for larger system sizes, as to eventually obtain information about their distribution.

Let us consider the single-particle Hamiltonian corresponding to the integrable many-body system of interest. This con-

tains hopping terms and possibly a background potential,

$$H = \sum_{i=1}^{L-1} (a_i^\dagger a_{i+1} + a_{i+1}^\dagger a_i) + \sum_{i=1}^L V_i a_i^\dagger a_i. \quad (8)$$

(The geometry could be something other than a chain, e.g., a 2D or 3D lattice, and the hoppings could be longer-range, without affecting any of the arguments below.) The creation/annihilation operators above can have any exchange statistics, for example, but not limited to, fermionic or bosonic.

The creation operators for the single-particle eigenstates are linear combinations of the a_i^\dagger operators,

$$d_k^\dagger = \sum_{j=1}^L \phi_j^{(k)} a_j^\dagger. \quad (9)$$

Here, $k = 1, \dots, L$ labels the single-particle eigenstates, and the j are site indices. The $\phi_j^{(k)}$ are single-particle eigenstate coefficients. For integrable systems, the many-body eigenstate coefficients are built out of these $\phi_j^{(k)}$ s.

In the simplest situation of nearest-neighbor hopping with no background potential, the $\phi_j^{(k)}$ are sine functions, e.g., with open boundary conditions,

$$\phi_j^{(k)} = \sqrt{\frac{2}{L+1}} \sin \frac{kj\pi}{L+1}. \quad (10)$$

In this case, the indices k can be interpreted as momenta. The corresponding single-particle energies are $E^{(k)} = 2 \cos \frac{k\pi}{L+1}$. The arguments below do not rely on a specific form of the single-particle eigenstates and energies.

For non-interacting bosons or fermions, the many-body eigenstates are constructed by filling the single-particle eigenstates with integer numbers of particles. The eigenstates can be labeled either as a list of occupancies of the L single-particle eigenstates,

$$|\tilde{n}_1, \dots, \tilde{n}_L\rangle = \prod_{k=1}^L \frac{1}{\tilde{n}_k!} (d_k^\dagger)^{\tilde{n}_k} |\text{vac}\rangle, \quad (11)$$

or as a list of the single-particle eigenstates occupied by the N particles,

$$|k_1, \dots, k_N\rangle = d_{k_1}^\dagger \cdots d_{k_N}^\dagger |\text{vac}\rangle. \quad (12)$$

Here $|\text{vac}\rangle$ is the vacuum (no particles in the system). The integers $\tilde{n}_k \geq 0$ indicate how many particles are in single-particle eigenstate $|k\rangle$. For fermions, $\tilde{n}_k = 0, 1$ and for bosons they can take values up to N . The many-body eigenenergy is equal to $\sum_{k=1}^L \tilde{n}_k E^{(k)}$.

For non-interacting bosons, the eigenstates can be expressed as the sum over permutations p of the positions (j_1, \dots, j_N) of the N particles. In the basis defined by the states $|j_1, \dots, j_N\rangle \equiv a_{j_1}^\dagger \cdots a_{j_N}^\dagger |\text{vac}\rangle$, the eigenstate coefficients are

$$\langle j_1, \dots, j_N | k_1, \dots, k_N \rangle = \frac{\sqrt{\gamma_{\{j\}}}}{\sqrt{\tilde{\gamma}_{\{k\}}}} \sum_{p \in \mathcal{P}} \phi_{p_1}^{(k_1)} \phi_{p_2}^{(k_2)} \cdots \phi_{p_N}^{(k_N)}, \quad (13)$$

where $\tilde{\gamma}_{\{k\}} = \prod_{k=1}^L \tilde{n}_k!$ and $\gamma_{\{j\}} = \prod_{j=1}^L n_j!$, and $p = (p_1, \dots, p_N)$ runs over all *distinct* permutations of the particle positions (j_1, \dots, j_N) . The summation may be conveniently implemented as the *permanent* per M of the $N \times N$ matrix M defined by $M_{ab} = \phi_{j_a}^{(k_b)}$ ($a, b = 1, \dots, N$).

For free fermions, the many-body eigenstates are linear combinations of the products of the single-particle eigenstates, as for free bosons. However, antisymmetry under exchange of particles introduces minus signs in this sum for odd permutations. The coefficients are therefore given by Slater determinants

$$\begin{aligned} \langle j_1, \dots, j_N | k_1, \dots, k_N \rangle \\ = \frac{1}{\sqrt{N!}} \det M = \frac{1}{\sqrt{N!}} \sum_{p \in \mathcal{P}} (-1)^p \phi_{p_1}^{(k_1)} \phi_{p_2}^{(k_2)} \cdots \phi_{p_N}^{(k_N)}. \end{aligned} \quad (14)$$

The single-particle eigenstates k_i are required to be distinct.

For systems solvable by the Bethe ansatz, the many-body amplitudes are also built out of single-particle coefficients. For the fermionic chain with nearest neighbor interactions (equivalent to the XXZ chain for present purposes),

$$\begin{aligned} \langle j_1, \dots, j_N | k_1, \dots, k_N \rangle \\ = \mathcal{N} \sum_{p \in \mathcal{P}} e^{i\chi(p)} \phi_{p_1}^{(k_1)} \phi_{p_2}^{(k_2)} \cdots \phi_{p_N}^{(k_N)}, \end{aligned} \quad (15)$$

where the phase shift $\chi(p) = \sum_{i < j} \chi_2(k_i, k_j)$ is interaction dependent and is a sum of two-particle phase shifts χ_2 , which are determined from the two-particle scattering problem. For more complicated models, such as those requiring the nested Bethe ansatz, the wavefunction is more involved, but the essential idea is the same.

C. Argument for power-law behavior — a toy model

We provide an argument for power-law behavior of the coefficient distribution by considering a toy model of N *distinguishable* particles, i.e., with trivial exchange statistics. In this case the multi-particle eigenfunction coefficients

$$c = \langle j_1, \dots, j_N | k_1, \dots, k_N \rangle = \prod_{i=1}^N \langle j_i | k_i \rangle = \prod_{i=1}^N \phi_{j_i}^{(k_i)}. \quad (16)$$

are merely products of values of the single-particle eigenstates $\phi_j^{(k)}$, where k label the eigenstates and j the site indices, cf. Eqs. (13)–(15). For N distinguishable particles in L sites, the Hilbert space dimension is $D = L^N$.

Because of the product-state nature of the coefficients c , it is natural to study the distributions $Q(y)$ of the logarithms

$$y = \log z = \log c + \log \sqrt{D}. \quad (17)$$

The distribution $Q(y)$ relates to the ‘usual’ coefficient distribution $P(z)$ as $Q(y) = e^y P(e^y)$ and $P(z) = \frac{1}{z} Q(\log z)$. The logarithm of the many-particle coefficients is the sum of the single-particle ones, $\log c = \sum_{i=1}^N \log \phi_{j_i}^{(k_i)}$, so that

$$y = \sum_{i=1}^N \log \phi_{j_i}^{(k_i)} + \frac{1}{2} N \log L. \quad (18)$$

If we regard the single-particle coefficients to be effectively random, then this is a sum of N random variables (plus a shift by a constant), and we can invoke the central limit theorem. It follows that $Q(y)$ at large N approaches a Gaussian distribution,

$$Q(y) \rightarrow \frac{1}{\sqrt{2\pi\sigma_Q^2}} e^{-(y-\mu_Q)^2/2\sigma_Q^2}, \quad (19)$$

with mean μ_Q and variance σ_Q^2 . The central limit theorem yields the mean to be the sum $\mu_Q = \sum_{i=1}^N \mu_{q_i}$ of the means μ_{q_i} of the single-particle log-coefficient distributions q_i of the variables $y_i = \log \phi_{j_i}^{(k_i)} + \frac{1}{2} \log L$ [i.e., one term in the sum of Eq. (18)]. The term $\frac{1}{2} \log L$ represents the scaling of the single-particle coefficients to unit variance, which renders the distributions q_i to be independent of system size in the limit $L \rightarrow \infty$. The values μ_{q_i} only depend on the lattice geometry and the quadratic couplings (e.g., short-range versus long-range couplings). Likewise, the variance σ_Q^2 approaches $\sum_{i=1}^N \sigma_{q_i}^2$ for large N , where the $\sigma_{q_i}^2$ are the variances of the single-particle distributions q_i .

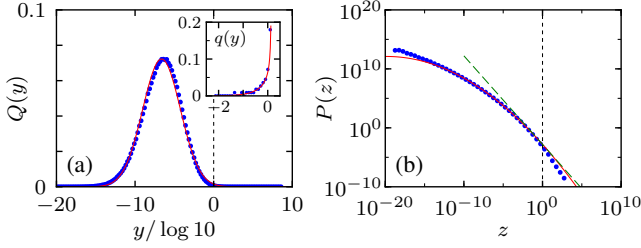


FIG. 5. (a) Distribution $Q(y)$ of the logarithms of the coefficients of the many-particle-in-a-box model, for $(L, N) = (100, 50)$. We consider a single eigenstate, with randomly chosen momenta (k_1, \dots, k_N) . The (blue) dots indicate the numerical result obtained by sampling 10^6 coefficients. The (red) curve is the estimated distribution Q from Eq. (19), with mean μ_Q and variance σ_Q^2 obtained from the single-particle distributions. The inset shows a typical single-particle distribution $q(y)$, with the dots and curve indicating the discrete and continuum distributions, respectively. (b) Corresponding coefficient distribution $P(z)$. The (green) dashed line is an estimate for the power law with exponent evaluated at $z = 1$.

The power-law behavior of $P(z) = \frac{1}{z} Q(\log z)$ now readily follows from studying the first- and second-order double-logarithmic derivative,

$$\frac{d \log P}{d \log z} = -\frac{\log z}{\sigma_Q^2} + \frac{\mu_Q}{\sigma_Q^2} - 1, \quad (20)$$

$$k = \frac{d^2 \log P}{d(\log z)^2} = -\frac{1}{\sigma_Q^2}. \quad (21)$$

Under the assumption of identical distributions $q_i = q$, we have $\sigma_Q^2 = N\sigma_q^2$ and $\mu_Q = N\mu_q$ and find that the second-order double-logarithmic derivative scales as $k \sim 1/N$. Thus, for increasing system size, the curvature of the coefficient distribution $P(z)$ on a double logarithmic scale decreases. In other words, $P(z)$ ‘flattens’ to a power law $\sim z^\alpha$. The exponent α of the power law follows from the first-order double-logarithmic derivative, $\alpha \rightarrow \mu_q/\sigma_q^2 - 1$ (at $z = 1$). The value is non-universal: it is determined by the details of the single-particle coefficient distributions.

In Fig. 5, we illustrate the effectiveness of this argument with the results for a model of many distinguishable particles in a finite chain with open boundary conditions (many particles in a box). The numerically obtained distribution fits well to the analytic estimate given by Eq. (19) with $\mu_Q = N\mu_q$ and $\sigma_Q^2 = N\sigma_q^2$. (In this case, the single-particle coefficient distributions are independent of the k_i ; they are all characterized by the same mean μ_q and variance σ_q^2 . We find $\mu_q \approx -0.347$ and $\sigma_q^2 \approx 0.822$, which yields the exponent $\alpha \approx -1.42$.) Small deviations may be seen in the tails, and the numerical distribution is slightly skewed to the right, due to the high asymmetry of the single-particle distribution q . These deviations vanish in the limit $N \rightarrow \infty$.

D. Extension to non-trivial statistics

From the data in Fig. 4, the question arises as of whether the preceding argumentation for a large- N approach to a power-law $P(z)$ can be extended naturally to indistinguishable particles with non-trivial statistics. For free bosons, free fermions and systems integrable through the Bethe ansatz, the eigenfunctions are not just products of single-particle wavefunctions, but linear combinations of them, as shown in Eqs. (13)–(15), respectively. At present, we are able to outline a partial argument only for the free-fermion case.

For free fermions, the many-body coefficients are determinants of the single-particle coefficients, Eq. (14). Assuming these coefficients to be effectively random, we invoke recent results from random matrix theory for the determinant of a random matrix [47, 48]. Assuming that the entries of a matrix A are essentially random, and their distribution is sufficiently well-behaved, $\log|\det A|$ satisfies a central-limit theorem: If the entries are distributed with zero mean and unit variance, the distribution of $\log|\det A|$ tends to a normal distribution for large N , with mean $\frac{1}{2} \log(N-1)!$ and variance $\frac{1}{2} \log N$. For our matrix M in Eq. (14), the entries are single-particle coefficients $\phi_j^{(k)}$ with variance $1/L$ by normalization. The matrix elements can be made to have unit variance by multiplying each element by \sqrt{L} , so that the determinant is multiplied by $(\sqrt{L})^N$. Thus, the coefficients are of the form

$$c = \frac{1}{\sqrt{N!}} \frac{1}{L^{N/2}} \det \tilde{M}, \quad (22)$$

where the matrix \tilde{M} now has entries with unit variance. Unfortunately, the entries do not necessarily have zero average; for example, if the coefficients are sinusoidal functions as in the case of an open-boundary chain, half of the single-particle coefficients have nonzero average. We proceed with the assumption that this nonzero average causes a shift ξ in the mean of the distribution of $\log|\det \tilde{M}|$, and leaves the variance unchanged. With this assumption, the variable $y = \log(c\sqrt{D})$ has a Gaussian distribution $Q(y)$, as in Eq. (19), with mean

$$\mu_Q = -\log \sqrt{N!} - \log L^{N/2} + \frac{1}{2} \log(N-1)! + \xi(N) + \log \sqrt{D} \quad (23)$$

and variance $\sigma_Q^2 = \frac{1}{2} \log N$.

Gaussianity of $Q(y)$ implies Eqs. (20) and (21) for the first- and second-order double-logarithmic derivative. The latter

$$k = -\frac{1}{\sigma_Q^2} = -\frac{1}{\frac{1}{2} \log N} \quad (24)$$

thus vanishes at large N . This signifies an approach to power-law form for $P(z)$ in the $N \rightarrow \infty$ limit. Compared to the product-type states, the convergence is slower: $k \sim -1/\log N_f$ [48]. This provides an appealing explanation to why we need enormous sizes to see the approach to power-law behavior, and is the reason we plot k against $1/\log N_f$ in Fig. 4(d), inset.

We now attempt to estimate the power-law exponent at large sizes. Equation (20) implies that the exponent is

$$\begin{aligned} \frac{\mu_Q}{\sigma_Q^2} - 1 &= \frac{-\frac{1}{2} \log N - \log L^{N/2} + \log \sqrt{D} + \xi(N)}{\frac{1}{2} \log N} - 1 \\ &= -2 + \frac{-\log L^{N/2} + \log \sqrt{D} + \xi(N)}{\frac{1}{2} \log N}. \end{aligned} \quad (25)$$

The fraction (second term) is N -dependent. (For the case of half-filling, $L = 2N$, the numerator is $-\frac{1}{2}N \log N + \xi(N)$ at large N .) For a sensible large- N limit, the N dependence must be canceled by the unknown shift $\xi(N)$. If the cancellation is perfect in the sense that the fraction vanishes, we obtain the estimate -2 for the exponent, i.e., the asymptotic power-law behavior $P(z) \propto z^{-2}$, which is consistent with the numerical data presented in Fig. 4. Of course, since we do not know the function $\xi(N)$, the fraction could also be an N -independent constant, in which case the exponent would be shifted from -2 .

The assumption that the nonzero average of the matrix elements leads only to a shift in the mean of $Q(y)$ seems quite reasonable. Proving such an assumption, or deriving $\xi(N)$, is well beyond the scope of the present work. The central limit theorem for log-determinants, invoked above, is cutting-edge mathematical work. We are not aware of mathematical results with modified conditions for the distribution of elements. Note, however, that a power-law dependence can be inferred under much weaker conditions than the assumption used above — as long as σ_Q^2 is an increasing function of N , we obtain a power-law $P(z)$ at large N .

At present, to our knowledge, no comparable central-limit-theorem analog is available for permanents [Eq. (13)] and certainly not for more complicated generalizations like Eq. (15) appearing in Bethe-ansatz wavefunctions, but a similar Gaussian limit for $Q(y)$, and hence a power-law $P(z)$ for large N , seems plausible. Thus, based on our numerical results and on the arguments above, a reasonable conjecture is that $P(z)$ approaches a power law *generically* in large-size integrable systems.

Any of these arguments (whether for trivial or for non-trivial statistics) rely on treating the single-particle logarithmic coefficients $\log \phi_a$ as independent random variables. While such an assumption is likely impossible to be ‘proved’, arguments in the same spirit underlie the eigenstate thermalization hypothesis (ETH) and its extensions [1–5, 37, 42, 49–51].

IV. QUANTUM BILLIARDS

In this section, we consider single-particle systems (‘billiards’) confined to a two-dimensional region either by a hard wall (Sec. IV A) or by a parabolic confining potential (Sec. IV B). We show that a number of integrable billiards have amplitude distributions with power-law tails, and present some data for systems with a mixed phase space.

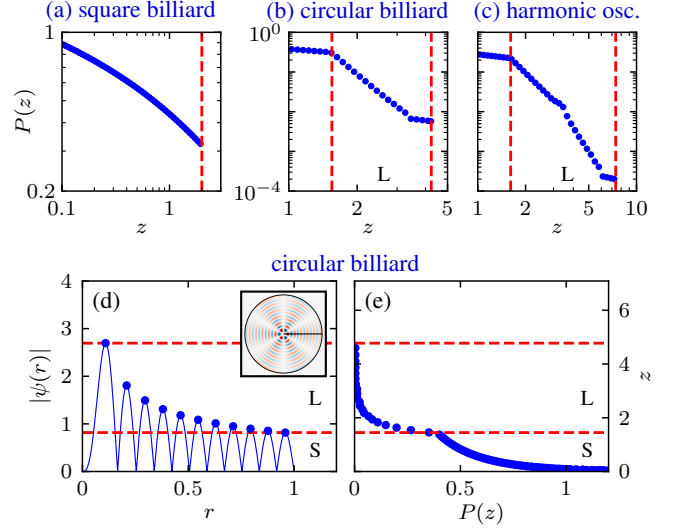


FIG. 6. Amplitude distributions in single-particle systems (log-log plots). Distributions shown for a single eigenstate of: (a) The square billiard, $\psi_{1,1}^\square$. (b) The circular billiard, $\psi_{101,37}^\circ$. (c) An anisotropic two-dimensional harmonic oscillator, $\psi_{141,121}^{\text{ho}}$. (d,e) Illustration of the origin of two distinct regimes (labeled S and L) of the amplitude distribution; here, for the circular billiard, eigenfunction $\psi_{3,11}^\circ$. In (d), the curve indicates $|\psi(r)|$ and the dots indicates local extrema. The inset visualizes $\psi_{3,11}^\circ(x, y)$. In (e), the resulting coefficient distribution is plotted sideways as function of z , which is scaled as to match the values of $|\psi(r)|$ in (d). In all panels, the red dashed lines indicate the ‘L’ regime, where power-law behavior can be expected. (For the square billiard, this regime is undefined.)

A. Hard walls

We now consider a single particle confined in a two-dimensional region Ω . The eigenfunctions $\psi_n(\vec{x})$, $\vec{x} = (x, y)$, satisfy the Schrödinger equation $-\nabla^2 \psi_n(\vec{x}) = E_n \psi_n(\vec{x})$ for $\vec{x} \in \Omega$, and vanish for $\vec{x} \notin \Omega$. Given an eigenstate $\psi(\vec{x})$ of a quantum billiard, we consider the probability distribution $P(z)$ of the (rescaled) absolute values z of the amplitudes, $z = |\psi(\vec{x})| \sqrt{\mathcal{A}}$, i.e.,

$$P(z)dz = \frac{1}{\mathcal{A}} \int_{z \leq |\psi(x,y)| \sqrt{\mathcal{A}} < z+dz} 1 dx dy. \quad (26)$$

Here, $\mathcal{A} = \text{area}(\Omega)$ is the area allowed by the billiard potential. Inclusion of the factor $\sqrt{\mathcal{A}}$ ensures that $P(z)$ has unit variance.

In contrast to chaotic quantum billiards, for which almost all eigenstates have Gaussian amplitude distributions [6–12, 14], we here investigate integrable billiards, as in [52]. The simplest case is the square billiard, whose eigenfunctions $\psi_{n_x n_y}^\square \propto \sin(n_x x) \sin(n_y y)$ all have the same amplitude distribution, which can be expressed analytically in terms of an elliptic integral (see Appendix C) and is shown in Fig. 6(a). The tail of the distribution, which originates from the peaks of the wavefunction, is $\sim z^{-1/2}$, but there is no extended power-law region. The circular billiard eigenstates ψ_{mn}° are labeled by angular and radial quantum numbers m and n . At

large n , the wavefunction has many oscillations in the radial direction, given by a Bessel function. This leads to a broad power-law segment in the amplitude distribution [see Fig. 6(b)]: $P(z) \sim z^{-\gamma}$, with $\gamma \approx 5$ for $n \gg 1$ (see Appendix C). The region extends from the height of the lowest peak to that of the highest peak, as illustrated by Figs. 6(d,e). In Fig. 6, the expected power-law regime, defined by the minimum and maximum peak amplitude, is indicated by the red dashed lines.

B. Soft walls

These results also extend to single-particle eigenstates of smooth confining potentials, i.e., with Hamiltonian $H = -\nabla^2 + V(x, y)$. In this case, we need to restrict the analysis of the distribution to the classically accessible region, and define \mathcal{A} [cf. Eq. (26)] to be the area of this region. Let us consider the 2D harmonic oscillator, $V_{\text{h.o.}}(x, y) = x^2 + \lambda^2 y^2$. The constant $\lambda = \frac{1}{2}(1 + \sqrt{5})$ is taken to be irrational in order to avoid complications with degeneracies. The eigenfunctions $\psi_{mn}^{\text{h.o.}}$ are products of the eigenfunctions of the one-dimensional harmonic oscillator, and have amplitude distributions with power-law tails. In Fig. 6(c), we illustrate the example $(m, n) = (141, 121)$. Like the circular billiard, this dependence arises due to a combination of many inequivalent peaks in the wavefunctions. The ‘kink’ in the power law regime at $z \approx 3$, that separates two regimes with different power law exponents, presumably stems from the product structure.

Generically, if the potential is modified, many eigenfunctions at higher energies look chaotic and have amplitude distributions with Gaussian tails. Typically, the phase space at higher energies is mainly chaotic, with small regular islands surrounding the short stable periodic orbits. Thus, in this regime, one typically encounters only a few regular eigenfunctions among many chaotic ones. In order to illustrate this observation, let us consider the weakly anharmonic potential $V(x, y) = x^2 + (\lambda y)^2 + \alpha x^2 y^2$, with $\alpha = 0.2$. In Fig. 7(a,b), we show an example of a chaotic eigenstate, whose amplitude distribution is Gaussian and whose eigenfunction is random-wave-like in a significant area of the classically accessible region. At nearly equal energy, we also find an example of a highly regular eigenfunction [Fig. 7(c,d)]; typically, such eigenfunctions have a large overlap with a small number of eigenstates of the non-perturbed model. The amplitude distribution typically shows power-law tails after a kink, much like the $|m, n\rangle$ themselves. Furthermore, there are “intermediate” eigenstates which have an extended wave function, but neither a power law nor a Gaussian fits well [Fig 7(e,f)].

V. CONTEXT & CONCLUSIONS

We have extended the study of amplitude distributions to many-body quantum systems. One context for this work is a growing appreciation that concepts from the field of single-particle quantum chaos can be useful for many-body quantum

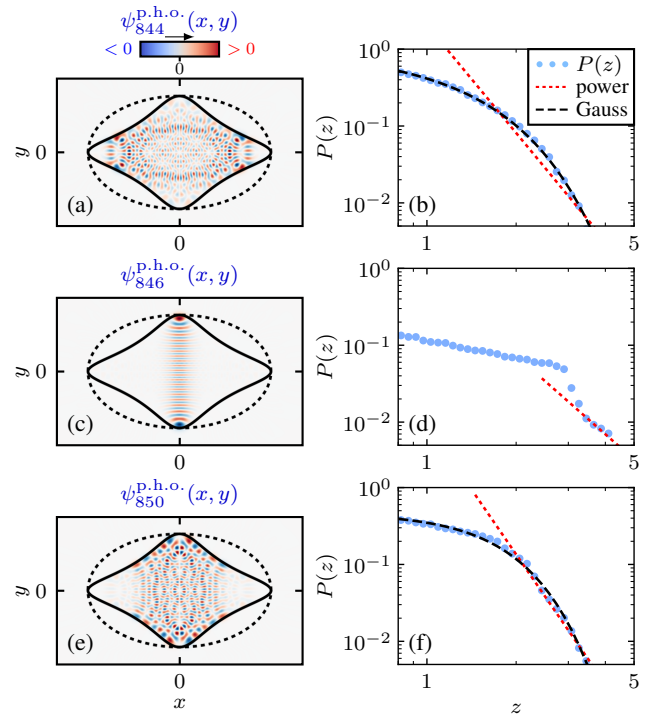


FIG. 7. Eigenstates of perturbed anisotropic 2D harmonic oscillator. The left-hand panels are wave functions $\psi_k^{\text{p.h.o.}}(x, y)$ (labeled $k = 0, 1, 2, \dots$ in increasing order of eigenvalues). The right-hand panels are double logarithmic plots of amplitude distributions $P(z)$ (blue points). We also indicate Gaussian and power law fits. In the wave-function plots, solid lines indicate the equipotential curve $V(x, y) = E^{(k)}$, and dotted elliptical lines indicate corresponding curves for the unperturbed potential. (a,b) For the state $\psi_{844}^{\text{p.h.o.}}$, $P(z)$ has a Gaussian tail. (c,d) The state $\psi_{846}^{\text{p.h.o.}}$, resembling a one-dimensional harmonic oscillator eigenstate, shows $P(z)$ features similar to that seen in integrable systems: a kink followed by an arguably power law tail. (e,f) State $\psi_{850}^{\text{p.h.o.}}$ is an intermediate state, whose tail fits neither a power law, nor a Gaussian, particularly well.

systems [1–5, 28, 29, 46, 53–58]. A global study of *all* many-body eigenstates, such as the present one, is not historically common in condensed matter physics. The full eigenspectrum has gained importance only recently, due to intense interest in the dynamics of isolated systems, including thermalization-related questions [1–5] and many-body localization [59, 60].

Our most striking result is the hint of a new type of universality associated with *integrable* many-body systems — the coefficient distribution approaches a power-law in the large-size limit. We have presented data and arguments to conjecture that this is a generic feature of multiple classes of integrable systems. Interestingly, we have shown that a number of regular single-particle billiards also show power-law tails in $P(z)$, although we do not claim this to be generic.

For non-integrable many-body systems, away from the spectral edges, we have found Gaussian amplitude distributions, as expected. An interesting feature is the slight deviation from Gaussianity in 1D geometries. Gaussian behavior is a measure for the randomness of eigenstates and thus

a characterization of non-integrable behavior; in this respect it complements other eigenstate properties such as entanglement randomness [42, 45], inverse PR [5, 28, 42, 46], phase correlators [61], ETH scaling [50, 62] etc. However, beyond its connection to chaos in eigenstates, we regard the coefficient distribution to be an object of basic importance in its own right.

This work raises a number of new questions:

(1) Ground states of many-body systems are multifractal [63, 64]. Multifractality is related to the moments of $P(z)$; hence in light of the present work one would like to investigate multifractality in the full spectrum. This requires modifying the definition in terms of size scaling, since there is no natural correspondence between eigenstates of different-sized systems. Appendix D provides some data on multifractality in a non-integrable many-body system.

(2) The distributions for eigenstates near the spectral edge are clearly not Gaussian (Fig. 1), but it is unclear whether there is any generic behavior, or a generic limiting distribution at large sizes.

(3) In (near-integrable) quantum billiards with a mixed phase space, the non-Gaussianity of $P(z)$ can sometimes be described by, e.g., modified Gaussians with position dependent variance [31]. For many-body systems, characterizing the non-Gaussianity of near-integrable eigenstates remains an open task.

(4) The basis dependence of the distributions is an open question. For example, in a mean-field basis [5] such as the eigenbasis of the XX ($\Delta = 0$) Hamiltonian, the integrable XXZ chain has a high-kurtosis non-Gaussian amplitude distribution, similar to the distribution in the coordinate basis [Fig. 1(b)].

Each of these questions points to interesting directions for future study.

Appendix A: Comments on Quantum Integrability

In classical mechanics, the notion of integrability is commonly understood to mean the presence of (at least) as many conserved quantities as the number of degrees of freedom (“Liouville-integrability”). In contrast, for quantum systems, there are a number of different notions of integrability, and it is possible to find exceptions to or inadequacies with most definitions. We briefly discuss here a few notions associated with integrability, so that the sense in which we have used the term is sufficiently clear.

Single-particle quantum billiard systems are called chaotic if the dynamics of the corresponding classical Hamiltonian system is chaotic. Conversely, a single-particle quantum system may be regarded as integrable or regular if the corresponding classical system has integrable (‘regular’) dynamics. When the integrability is broken, the system typically has a so-called mixed phase space, consisting of regions with regular motion and regions with chaotic motion. This is reflected in the quantum eigenstates which are typically concentrated either within the regular regions or the chaotic regions.

For quantum many-body systems, the situation is substantially more complicated [15, 16]. Let us first consider systems where a large-size (‘thermodynamic’) limit is naturally defined. For example, this includes fermionic or bosonic systems, where the limit is defined by increasing the system size while keeping the density constant, and magnetic systems where the limit is defined by increasing the system size while keeping the magnetization density constant. In such cases, the Hilbert-space dimension increases exponentially with system size. A common notion of integrability is that, if the system can be ‘solved’ with polynomial rather than exponential effort, then the system is integrable. Here, ‘solving’ means finding the eigenvalues and eigenstates of the Hamiltonian. For example, for systems of non-interacting fermions or bosons, it is sufficient to find the eigenvalues and eigenstates of the single-particle problem; this allows construction of the many-body eigenstates. For systems solvable by the Bethe ansatz, the problem can be reduced to a polynomial number of nonlinear equations. In the simpler examples of the Bethe ansatz, such as the XXZ chain, the number of equations is equal to the number of particles. For more complicated cases, such as those requiring a nested Bethe ansatz solution, the counting is more complicated, but the basic idea of polynomial solvability still applies.

The idea of polynomial solvability is closely related to the physical idea that an integrable system has a macroscopic number of conserved quantities. The number of conserved quantities scales polynomially (generally linearly) with the system size. The conserved quantities for non-interacting fermions/bosons are the occupancies of single-particle modes. For systems integrable only via the Bethe ansatz, the conserved quantities are often difficult to construct explicitly, although their existence is guaranteed.

It is interesting to note that the above notion of integrability relies on large-size scaling, and thus strictly speaking is not defined for a single fixed-size system, which is in sharp contrast to the single-particle billiard case. However, if a many-body Hamiltonian is integrable, then a ‘reasonably large’ system will show Poissonian level statistics. While this is a phenomenological statement and not very rigorous, it is sufficient for many purposes, and we can thus consider the level statistics to provide an operational distinction between integrable and non-integrable many-body systems. The advantage of this viewpoint is that one can discuss integrability in both single-particle quantum billiards and in many-body systems within the same framework. Note, however, that even for the single-particle case there are integrable systems not following Poissonian statistics; these are usually considered as “non-generic”.

There are various situations where the setup assumed here is not appropriate. For example, there are single-impurity problems which are solvable by Bethe ansatz, such as the Kondo model, the Anderson impurity model, and the interacting resonant level model. In these cases, a constant-density scaling is not natural, as the impurity is localized in space. In addition, these models are generally integrable only for linearized bath dispersions, and the high-energy spectrum of the linearized models may not be very physical. Another unclear

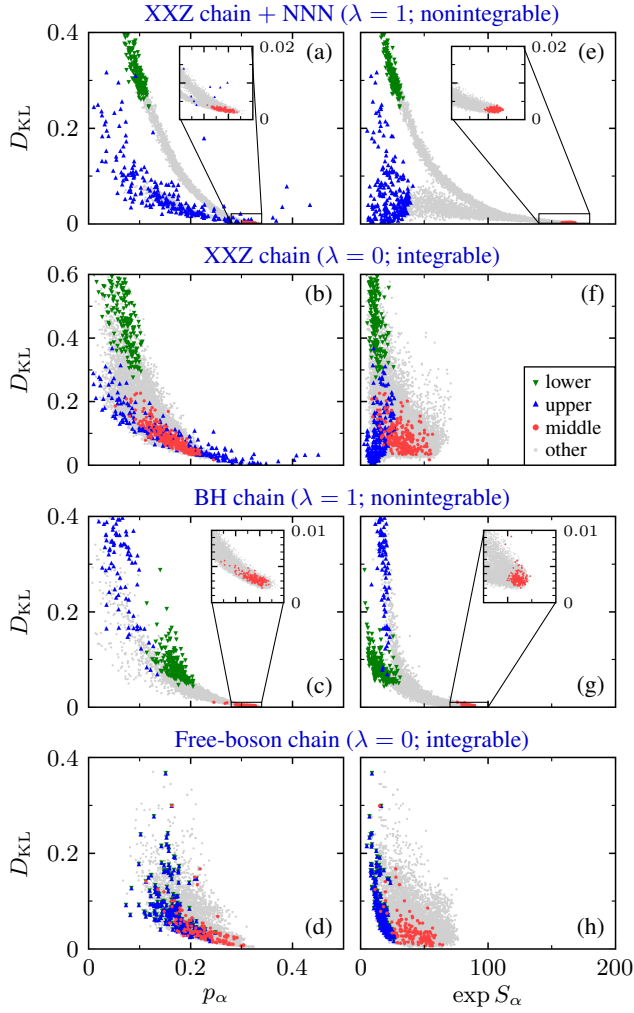


FIG. 8. Kullback-Leibler divergence plotted against participation ratio (a)–(d) and against entanglement entropy with respect to left-right partition (e)–(h). We show data for the XXZ chain with and without NNN coupling, and for the boson chain with and without Hubbard interaction. The system sizes are $(L, N_\uparrow) = (17, 8)$ and $(L, N_b) = (13, 6)$, respectively. In all cases, we have highlighted 250 states at the lower and upper edge of the spectrum and in the middle.

situation involves zero-dimensional models, such as the two-site Bose-Hubbard model. Although the solution of this model can be written in Bethe ansatz form, the ansatz does not reduce an exponential problem, because the Hilbert space has polynomial size to begin with (growing linearly with the particle number). In this work, we have ignored such special situations and restricted to many-body models where a clean and natural thermodynamic limit can be defined.

Appendix B: Entanglement entropy, participation ratio, and deviations from Gaussianity

In this Appendix we present data showing how the entanglement entropy (EE), the participation ratio (PR) and the de-

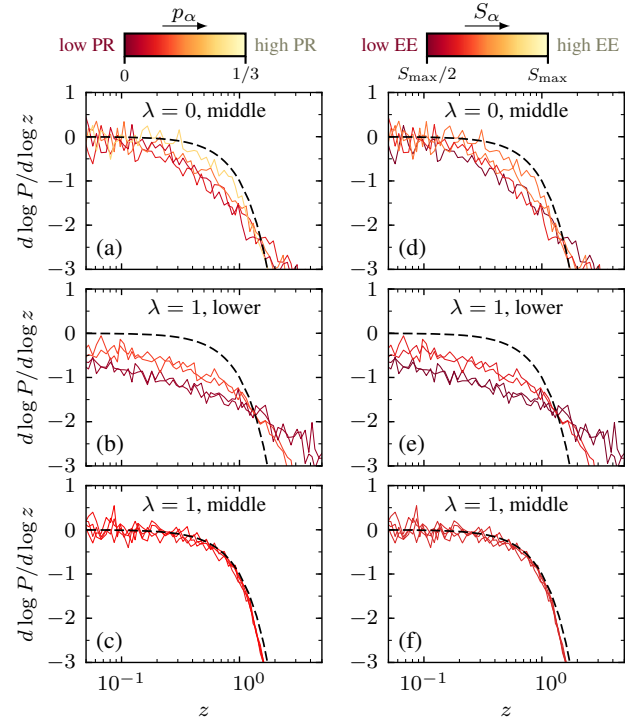


FIG. 9. Double-logarithmic derivative of the coefficient distribution for 4 individual eigenstates. (a,d) Integrable XXZ chain, middle of spectrum (near $E = 0$). (b,e) Non-integrable XXZ chain, lower end of spectrum. (c,f) Non-integrable XXZ chain, middle of spectrum. Left column (a,b,c): Colors (shading) indicate values P_α of the PR. The PR ranges from $P_\alpha = 0$ to $P_\alpha = 1/3$. (d,e,f): The same distributions, but with the color (shading) representing EE values S_α . Values range from $S_{\max}/2$ to S_{\max} , where $S_{\max} = 8 \log 2$ is the maximum possible entropy. The dashed curves indicate the Gaussian distribution.

viation from Gaussianity (quantified using the KLD) are correlated.

We first present scatter-plots (one data point for each eigenstate) allowing visualization of the degree of correlation. Figures 8(a)–(d) show plots of PR versus KLD for all eigenstates, for the XXZ chain with and without NNN coupling, and for the bosonic model with and without interaction. Analogously, we show in Figs. 8(e)–(h) the correlation between the KLD and $\exp(S_\alpha)$, where S_α is the EE with respect to a partition of the system into two connected parts of sizes l and $l + 1$, where $2l + 1 = L$. As argued in Sec. II, there is strong correlation visible in the non-integrable case [Figs. 8(a), (c), (e), and (g)]: a large deviation from Gaussianity is associated with small PR and with small EE between spatial partitions. The correlation is less clear in the integrable cases [Figs. 8(b), (d), (f), and (h)], similar to previous findings for the correlation between EE and PR in eigenstates [42].

Next, in Fig. 9, we plot the double-logarithmic derivative of the coefficient distributions for some of the individual eigenstates. We have plotted the distributions of $c_\gamma^{(\alpha)}$ of four individual representatives close to the designated part of the spectrum. The chosen states are the highest-PR, lowest-PR,

highest-EE, and lowest-EE eigenstates within each group of 250 eigenstates.

Comparing the curves, we observe a clear correlation between the shape of the distribution and the PR and EE: The curves that lie closest to the Gaussian, e.g., for the non-integrable model in the middle of the spectrum [Figs. 9(c) and (f); cf. Figs. 8(b) and (f)] are high-PR and high-EE states, as seen from the coloring (shading). The other (flatter, more power-law like) curves are low-PR and low-EE states. For the non-integrable model, the eigenstates close to the lower edge of the spectrum show integrable behavior. This situation, shown in Figs. 9(b) and (e) is very similar to generic eigenstates in the integrable system [Figs. 9(a) and (d)]. On the other hand, in the bulk of the non-integrable spectrum [Figs. 9(c) and (f)], all eigenstates have nearly Gaussian coefficient distributions, and this is also reflected by the small variation in EE and PR. With the KLD as a measure of distance to Gaussian, these observations are consistent with those of Figs. 8(a), (b), (e), and (f).

Appendix C: Quantum billiards — analytical observations

In this Appendix, we provide some analytical results on amplitude distributions for the single-particle (‘quantum billiard’) systems described in Sec. IV, namely, the square billiard and the circular billiard.

1. Square billiard

For the billiard in a square $\{(x, y) \mid 0 \leq x, y \leq 1\}$ (so that $\mathcal{A} = 1$) with Dirichlet boundary conditions, the wave functions are given by

$$\psi_{mn}^\square(x, y) = 2 \sin(m\pi x) \sin(n\pi y) \quad (\text{C1})$$

with eigenenergies $\pi^2(m^2 + n^2)$. The coefficient distribution is independent of m and n , so we choose the ground state $m = n = 1$ for simplicity and without loss of generality.

We present a derivation of $P(z)$ as the z derivative of the area of the region defined by $\psi_{11}(x, y) < z$. We first simplify the problem by studying the function $f(x, y) = \cos x \cos y$ (with $|x|, |y| \leq \pi/2$), which is a scaled and shifted version of the wave function $\psi_{11}(x, y)$. The region defined by $f(x, y) > c$ encloses an area $A(c)$ complementary to the one we desire to compute. Considering the area in the first quadrant ($x \geq 0, y \geq 0$) only, we find

$$\frac{1}{4}A(c) = \int_0^{\arccos c} dy \arccos(c/\cos y), \quad (\text{C2})$$

using that the boundary is given by $x = \arccos(c/\cos y)$, and y runs from 0 to $\arccos c$. Substitution $w = \cos y$, such that $dy = -dw/\sqrt{1-w^2}$, yields the integral

$$\frac{1}{4}A(c) = \int_c^1 \frac{dw}{\sqrt{1-w^2}} \arccos(c/w). \quad (\text{C3})$$

The solution to our initial problem, namely, the size of the level set defined by $z = \psi_{11}(x, y)$, is proportional to the derivative of $A(z/2)$, with a scaling factor $1/\pi^2$. By computation of the derivative of Eq. (C3), we obtain

$$P(z) = -\frac{1}{\pi^2} \frac{d}{dz} [A(z/2)] = \frac{2}{\pi^2} K \left(\sqrt{1 - (z/2)^2} \right), \quad (\text{C4})$$

where $K(k) = \int_0^1 (1-t^2)^{-1/2} (1-k^2 t^2)^{-1/2} dt$ denotes the complete elliptic integral of the first kind.

From this expression, we find the approximate behavior $\sqrt{2/\pi^2 z}$ near the maximum value $z = 2$, i.e., a scaling $\sim z^{-\gamma}$ with $\gamma = \frac{1}{2}$. There is however no extended power-law behavior. Equation (C4) also shows that the coefficient distribution diverges for $z \rightarrow 0$.

2. Circular billiard

For the circular billiard of radius 1 (with $\mathcal{A} = \pi$), the eigenstates of the Hamiltonian $H = -\nabla^2$ are given in polar coordinates r, ϕ by

$$\psi_{mn}^\circ(\vec{r}) = \mathcal{N}_{mn} J_m(j_{mn} r) \cos(m\phi) \quad (\text{C5})$$

where J_m is the Bessel function of the first kind of integer order $m \geq 0$, j_{mn} is the n 'th zero of this function ($n > 0$ integer), and

$$\mathcal{N}_{mn}^2 = \begin{cases} 2/[\pi J_{m-1}(j_{mn})^2] & (m > 0) \\ 1/[\pi J_1(j_{0n})^2] & (m = 0) \end{cases} \quad (\text{C6})$$

is the normalization factor. The energy eigenvalue of this state is j_{mn}^2 .

The amplitude distribution $P(z)$ has a power-law tail when the radial quantum number n is large, i.e., the eigenfunction has many oscillations in the radial direction. The method of obtaining $P(z)$ can be illustrated using Figs. 6(d,e). The value $P(z)dz$ is proportional to the area of the region where $|\psi(\vec{r})| \in (c, c+dc)$, with $c = z/\sqrt{\mathcal{A}} = z\pi^{-1/2}$, is satisfied. For a one-dimensional function $\psi(r)$, $P(z)$ is thus given by the sum over $1/|\psi'(r_i)|$ over all solutions $\psi(r_i) = c$.

As already addressed in Sec. IV, Figs. 6(d,e) also visualize two distinct regimes: For small z , $|\psi(r, 0)| = c = z\pi^{-1/2}$ has a fixed number of solutions, and the coefficient distribution is thus determined by the derivatives. For larger z , the coefficient distribution is also affected by the number of solutions, which gradually decreases if z is increased. The boundary between these regimes is the value of the smallest local maximum of $|\psi|$.

We will now focus on the limit of $m = 0$ and large n . For large arguments x , the Bessel function $J_m(x)$ behaves as an oscillatory function with amplitude $\sim x^{-1/2}$. More specifically (e.g., Eq. 9.2.1 of Ref. [65]),

$$J_m(x) = \sqrt{\frac{2}{\pi x}} \left[\cos\left(x - m\frac{\pi}{2} - \frac{\pi}{4}\right) + \mathcal{O}(|x|^{-1}) \right]. \quad (\text{C7})$$

Given that n is large, the argument $j_{0n}r$ in the Bessel function is large except for small r . The contribution from $r \rightarrow 0$

is suppressed due to the geometry (Jacobian of polar coordinates); therefore it is reasonable to use the above large- $j_{0n}r$ approximation. Thus

$$\begin{aligned}\psi_{0n}^o(\vec{r}) &\approx \sqrt{\frac{1}{\pi J_1(j_{0n})^2}} \sqrt{\frac{2}{\pi j_{0n}r}} \cos(j_{0n}r - \frac{\pi}{4}) \\ &\approx \sqrt{\frac{1}{\pi r}} \cos(n\pi r - \frac{\pi}{4}r - \frac{\pi}{4}),\end{aligned}\quad (C8)$$

where we have used $j_{0n} \approx (n - \frac{1}{4})\pi$ and $\pi J_1(j_{0n})^2 \approx 2/j_{0n}$ according to approximation (C7).

Small z — We first derive the behavior of $P(z)$ of $\psi_{0,n}^o$ for small z . For $z = 0$, we sum over all contributions where the wave function intersects zero. For this purpose, we find the derivative

$$\begin{aligned}\psi_{0n}'(r) &= -\frac{1}{2}\pi^{-1/2}r^{-3/2} \cos(n\pi r - \frac{\pi}{4}r - \frac{\pi}{4}) \\ &\quad - r^{-1/2}(n - \frac{1}{4})\pi^{1/2} \sin(n\pi r - \frac{\pi}{4}r - \frac{\pi}{4})\end{aligned}\quad (C9)$$

with respect to r . Let us label the zeros of ψ_{0n} by $r_k = j_{0k}/j_{0n} \approx (k - \frac{1}{4})/(n - \frac{1}{4})$ with $k = 1, \dots, n$. At $r = r_k$, the cosine term vanishes and the sine term is of unit magnitude, so that we find

$$\begin{aligned}|\psi_{0n}'(r_k)| &= \sqrt{\pi/r_k}(n - \frac{1}{4}) \approx \sqrt{\pi}(n - \frac{1}{4})^{3/2}(k - \frac{1}{4})^{-1/2} \\ &\approx \sqrt{\pi n^3/k}.\end{aligned}\quad (C10)$$

Summing over all zeros, the contribution to the coefficient distribution becomes (in approximation)

$$2 \sum_{k=1}^n 2\pi r_k / |\psi_{0n}'(r_k)| \sim \sum_{k=1}^n \frac{k}{n} \frac{k^{1/2}}{n^{3/2}} = \sum_{k=1}^n \frac{k^{3/2}}{n^{5/2}} \sim 1. \quad (C11)$$

From this result, we deduce that the coefficient distribution has a finite value near 0. We find the form $P(z) \approx \alpha + \beta z^2$ for small z with $\alpha = \frac{8}{5}\sqrt{\pi}$ and $\beta > 0$. The vanishing of the linear term in z can be understood from a symmetry argument on the coefficient distribution of ψ_{0n} , rather than of $|\psi_{0n}|$.

Large z — When z is larger than the smallest maximum, the number of intersections defined by $\psi_{0n}(r) = c = z\pi^{-1/2}$ depends on the value of z . The maxima of $|\psi_{0n}(r)|$ are found at $r'_k \approx (k + \frac{1}{4})/(n - \frac{1}{4})$ and are characterized by $|\psi_{0n}(r'_k)| \approx \sqrt{1/\pi r'_k} \approx \sqrt{n/k\pi}$. The number of intersections is twice the number of maxima with $|\psi_{0n}(r'_k)| \geq z$, i.e., $2k_{\max}$ with $k_{\max} = \lfloor n/\pi z^2 \rfloor$. At the intersection points the derivatives are also roughly of the order $n^{3/2}k^{-1/2}$ (assuming that the sine term dominates, which is true for $r \gg 1/n$, i.e., almost all k except the smallest ones). Then, performing a similar summation as above, we obtain

$$\begin{aligned}2 \sum_{k=1}^{k_{\max}} 2\pi r'_k / |\psi_{0n}'(r'_k)| &\sim \sum_{k=1}^{k_{\max}} \frac{k^{3/2}}{n^{5/2}} \sim k_{\max}^{5/2}/n^{5/2} \\ &\sim (n/c^2)^{5/2}/n^{5/2} = c^{-5} \propto z^{-5}.\end{aligned}\quad (C12)$$

This scaling is valid for $z \gtrsim 1$ ($c \gtrsim \sqrt{1/\pi} \approx 0.56$), but the approximation becomes worse for large z , i.e., if $z \sim \sqrt{n}$

($c \sim \sqrt{n/\pi}$). Numerical data (e.g., as shown in Fig. 6) agrees with this finding: The coefficient distribution shows a power-law scaling $\alpha z^{-\gamma}$ with $\gamma \approx 5$, with a deviation of less than 0.05 for large n . (For example, $n = 301$ yields $\gamma = -4.96 \pm 0.05$.) The multiplicative constant α is almost independent of n , because the coefficient distribution converges for $n \rightarrow \infty$: In this limit the zeros and maxima of $|\psi_{0n}|$ become denser, but the envelope remains unaltered, cf. Eq. (C7).

For large n and nonzero but small m , the numerical results show a similar scaling $z^{-\gamma}$, where γ is close to 5. The $\cos(m\phi)$ argument does not alter the overall derivation outlined above.

Appendix D: Multifractality

The moments of the coefficient distribution are used to define multifractality of wavefunctions. It is known that ground states of many-body systems are generally multifractal [63, 64]. We consider here extending this idea to the full spectrum. Following Ref. [63], we define multifractality in terms of the Rényi entropies obtained from the many-body wavefunction coefficients c_γ ,

$$S_R(q, D) = -\frac{1}{q-1} \log \left(\sum_{\gamma=1}^D |c_\gamma|^{2q} \right). \quad (D1)$$

The summation runs from 1 to D , the Hilbert space dimension. Then the fractal dimensions are defined as

$$\mathcal{D}_q = \lim_{D \rightarrow \infty} \frac{S_R(q, D)}{\log D}. \quad (D2)$$

Wavefunctions are *multifractal* if the fractal dimension \mathcal{D}_q depends on the Rényi parameter q . They are simply *fractal* if \mathcal{D}_q is a constant other than 1. For Gaussian wavefunctions, they are expected to be constant at $\mathcal{D}_q = 1$. Thus, we expect a difference in scaling behavior between the spectral edges and the mid-spectrum eigenstates. However, except for the ground state and the highest-energy state, it is not clear that there is a meaningful comparison between sizes—an eigenstate for $L = 13$ cannot in general be unambiguously associated with an eigenstate of the $L = 15$ system. The $D \rightarrow \infty$ limit in the definition is thus not *a priori* well-defined.

In Fig. 10 we display scaled Rényi entropies for the non-integrable spin chain defined in Eq. (1), with $\lambda = 1$ and $\Delta = 0.8$. We plot $S_R(q, D)/\log D$, for the ground state, for four states near the middle of the spectrum, and for the topmost (highest-energy) state. In each case, three different system sizes are compared.

The ground states and the topmost state of successive system sizes can be meaningfully compared, and the limit in the definition of \mathcal{D}_q is unambiguous. Both these cases [Figs. 10(a) and (c)] have almost converged already; extrapolation will give a q -dependent fractal dimension. Hence these non-Gaussian states are multifractal. For the ground state, this is consistent with the findings of Ref. [63].

For other eigenstates, the limiting procedure is not well-defined, as explained above. Here, we simply take several

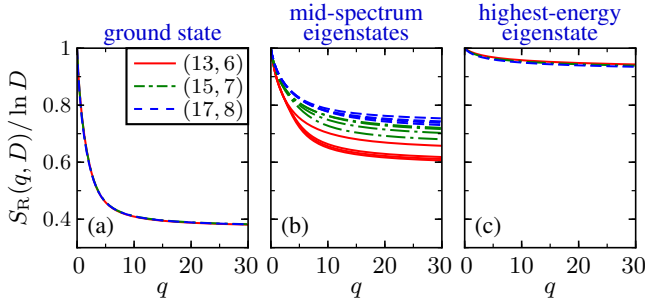


FIG. 10. Scaled Rényi entropies $S_R(q, D)/\log D$ for (a) the ground state, (b) four mid-spectrum states, and (c) the highest-energy eigenstate of the XXZ model with NNN couplings. We compare three system sizes (L, N_\uparrow) , with $N_\uparrow = 6, 7, 8$ up-spins in $L = 2N_\uparrow + 1$ sites; see the legend.

eigenstates from near the center of the spectrum for each size, Fig. 10(b). The trend as the size increases is consistent with the expected non-fractal behavior ($\mathcal{D}_q = 1$). However, the approach toward $\mathcal{D}_q = 1$ (assuming there is such an approach) is quite slow. Also, there are significant eigenstate-to-eigenstate fluctuations.

In summary, the data is consistent with the idea that the eigenstates are multifractal at the spectral edges and non-fractal in the middle of the spectrum, but the limit is not unambiguously defined and would be computationally challenging to characterize completely.

ACKNOWLEDGMENTS

We thank A. Chandran, M. Heyl, I. Khaymovich, A. Lakshminarayan, C. R. Laumann, and L. Santos for discussions.

-
- [1] J. M. Deutsch, Phys. Rev. A **43**, 2046 (1991).
 - [2] M. Srednicki, Phys. Rev. E **50**, 888 (1994).
 - [3] M. Rigol, V. Dunjko, and M. Olshanii, Nature **452**, 854 (2008).
 - [4] L. D'Alessio, Y. Kafri, A. Polkovnikov, and M. Rigol, Adv. Phys. **65**, 239 (2016).
 - [5] F. Borgonovi, F. M. Izrailev, L. F. Santos, and V. G. Zelevinsky, Phys. Rep. **626**, 1 (2016).
 - [6] M. Shapiro and G. Goelman, Phys. Rev. Lett. **53**, 1714 (1984).
 - [7] S. W. McDonald and A. N. Kaufman, Phys. Rev. A **37**, 3067 (1988).
 - [8] R. Aurich and F. Steiner, Physica D **48**, 445 (1991).
 - [9] R. Aurich and F. Steiner, Physica D **64**, 185 (1993).
 - [10] B. Li and M. Robnik, J. Phys. A: Math. Gen. **27**, 5509 (1994).
 - [11] F. Simmel and M. Eckert, Physica D **97**, 517 (1996).
 - [12] T. Prosen, Phys. Lett. A **233**, 332 (1997).
 - [13] A. Bäcker, in *The Mathematical Aspects of Quantum Maps*, Lecture Notes in Physics, Berlin Springer Verlag, Vol. 618, edited by M. D. Esposti and S. Graffi (2003) pp. 91–144, arXiv:nlin/0204061.
 - [14] A. Bäcker, Eur. Phys. J. Special Topics **145**, 161 (2007).
 - [15] B. Sutherland, *Beautiful Models: 70 Years of Exactly Solved Quantum Many-body Problems* (World Scientific, 2004).
 - [16] J.-S. Caux and J. Mossel, J. Stat. Mech. **2011**, P02023.
 - [17] O. Bohigas, M. J. Giannoni, and C. Schmit, Phys. Rev. Lett. **52**, 1 (1984).
 - [18] M. V. Berry and M. Tabor, Proc. R. Soc. A **356**, 375 (1977).
 - [19] G. Montambaux, D. Poilblanc, J. Bellissard, and C. Sire, Phys. Rev. Lett. **70**, 497 (1993).
 - [20] D. Poilblanc, T. Ziman, J. Bellissard, F. Mila, and G. Montambaux, Europhys. Lett. **22**, 537 (1993).
 - [21] T. C. Hsu and J. C. Anglès d'Auriac, Phys. Rev. B **47**, 14291 (1993).
 - [22] D. A. Rabson, B. N. Narozhny, and A. J. Millis, Phys. Rev. B **69**, 054403 (2004).
 - [23] A. R. Kolovsky and A. Buchleitner, Europhys. Lett. **68**, 632 (2004).
 - [24] K. Kudo and T. Deguchi, J. Phys. Soc. Jpn **74**, 1992 (2005).
 - [25] J. Karthik, A. Sharma, and A. Lakshminarayan, Phys. Rev. A **75**, 022304 (2007).
 - [26] L. F. Santos, J. Math. Phys. **50**, 095211 (2009).
 - [27] C. Kollath, G. Roux, G. Biroli, and A. M. Läuchli, J. Stat. Mech. **2010**, P08011.
 - [28] L. F. Santos and M. Rigol, Phys. Rev. E **81**, 036206 (2010).
 - [29] L. F. Santos, F. Borgonovi, and F. M. Izrailev, Phys. Rev. E **85**, 036209 (2012).
 - [30] Y. Y. Atas, E. Bogomolny, O. Giraud, and G. Roux, Phys. Rev. Lett. **110**, 084101 (2013).
 - [31] A. Bäcker and R. Schubert, J. Phys. A: Math. Gen. **35**, 527 (2002).
 - [32] E. J. Heller, Phys. Rev. Lett. **53**, 1515 (1984).
 - [33] A. Bäcker, R. Schubert, and P. Stifter, J. Phys. A: Math. Gen. **30**, 6783 (1997).
 - [34] M. V. Berry, J. Phys. A: Math. Gen. **10**, 2083 (1977).
 - [35] C. E. Porter and R. G. Thomas, Phys. Rev. **104**, 483 (1956).
 - [36] D. J. Luitz and Y. Bar Lev, Phys. Rev. Lett. **117**, 170404 (2016).
 - [37] R. Mondaini and M. Rigol, Phys. Rev. E **96**, 012157 (2017).
 - [38] R. Mondaini, K. R. Fratus, M. Srednicki, and M. Rigol, Phys. Rev. E **93**, 032104 (2016).
 - [39] Y. Y. Atas and E. Bogomolny, J. Phys. A: Math. Gen. **50**, 385102 (2017).
 - [40] S. Kullback and R. A. Leibler, Ann. Math. Statist. **22**, 79 (1951).
 - [41] Here, we separate the system in two spatial parts A and B of (nearly) equal size. Given a state $|\psi\rangle$, the entanglement entropy is $S = -\text{Tr} \rho_A \log \rho_A$, where $\rho_A = \text{Tr}_B |\psi\rangle\langle\psi|$ is the reduced density matrix. The spatial partition is most relevant to the present study of amplitudes in the basis of real-space configurations.
 - [42] W. Beugeling, A. Andreanov, and M. Haque, J. Stat. Mech. **2015**, P02002.
 - [43] V. Alba, M. Fagotti, and P. Calabrese, J. Stat. Mech. **2009**, P10020.
 - [44] J. R. Garrison and T. Grover, Phys. Rev. X **8**, 021026 (2018).
 - [45] L. Vidmar and M. Rigol, Phys. Rev. Lett. **119**, 220603 (2017).
 - [46] L. F. Santos and M. Rigol, Phys. Rev. E **82**, 031130 (2010).
 - [47] T. Tao and V. Vu, Adv. Math. **231**, 74 (2012).
 - [48] H. H. Nguyen and V. Vu, Ann. Probab. **42**, 146 (2014).
 - [49] C. Neuenhahn and F. Marquardt, Phys. Rev. E **85**, 060101 (2012).

- [50] W. Beugeling, R. Moessner, and M. Haque, Phys. Rev. E **89**, 042112 (2014).
- [51] W. Beugeling, R. Moessner, and M. Haque, Phys. Rev. E **91**, 012144 (2015).
- [52] R. Samajdar and S. R. Jain, J. Math. Phys. **59**, 012103 (2018).
- [53] M. Horoi, V. Zelevinsky, and B. A. Brown, Phys. Rev. Lett. **74**, 5194 (1995).
- [54] V. Zelevinsky, B. A. Brown, N. Frazier, and M. Horoi, Phys. Rep. **276**, 85 (1996).
- [55] V. V. Flambaum, F. M. Izrailev, and G. Casati, Phys. Rev. E **54**, 2136 (1996).
- [56] V. V. Flambaum and F. M. Izrailev, Phys. Rev. E **56**, 5144 (1997).
- [57] T. Guhr, A. Müller-Groeling, and H. A. Weidenmüller, Phys. Rep. **299**, 189 (1998).
- [58] M. Rigol and L. F. Santos, Phys. Rev. A **82**, 011604 (2010).
- [59] R. Nandkishore and D. A. Huse, Annu. Rev. Condens. Matter Phys. **6**, 15 (2015).
- [60] E. Altman and R. Vosk, Annu. Rev. Condens. Matter Phys. **6**, 383 (2015).
- [61] J. R. Armstrong, S. Åberg, S. M. Reimann, and V. G. Zelevinsky, Phys. Rev. E **86**, 066204 (2012).
- [62] M. Haque and P. McClarty, ArXiv e-prints (2017), arXiv:1711.02360 [cond-mat.stat-mech].
- [63] Y. Y. Atas and E. Bogomolny, Phys. Rev. E **86**, 021104 (2012).
- [64] D. J. Luitz, F. Alet, and N. Laflorencie, Phys. Rev. Lett. **112**, 057203 (2014).
- [65] M. Abramowitz and I. A. Stegun, *Handbook of Mathematical Functions*, Dover Books on Mathematics (Dover Publications, 1972).